Progress In Electromagnetics Research B, Vol. 85, 163–180, 2019

Optimization and Additive Manufacture of a Miniature 3-D Pixel Antenna for Dual-Band Operation

Germán A. Ramírez Arroyave* **and Javier L. Araque Quijano**

Abstract—This paper presents the design, manufacture, and experimental validation of a novel 3-D pixel antenna with volume-filling characteristics, and the design is based on our Method of Moments (MoM) solver that is efficiently coupled with a global/local optimizer for tailoring the antenna shape and concurrently selecting the location of the feeding port and shorting straps. The design, aimed at operating in the ISM bands of 2.45 GHz and 5.8 GHz, has dimensions under one-tenth of wavelength at the lowest frequency of operation. The optimization results are cross-validated using a commercial full-wave simulator, with a deviation of the reflection coefficient across the operating bands within 3%, showing also a high antenna efficiency of 99.6% and a gain of 1.06 and 4.53 dBi at the matching frequencies, with radiation patterns predominantly oriented towards the top hemisphere. Tolerance and parameter sensitivity studies were also performed. A scaled-up prototype of the antenna was built at a very low cost using standard additive manufacturing techniques, featuring a very good agreement between simulation and measurements, which proves the feasibility of this new kind of complex shape antennas in further applications where compact internal antennas are required.

1. INTRODUCTION

Additive Manufacturing (AM) is revolutionizing several fields of engineering [1, 2], not only as a prototyping technique but seriously envisioned as an alternative for small-scale production of customized and complex shaped devices [3] in what is called Direct Digital Manufacturing (DDM).

AM [4] is a term that encompasses a series of manufacturing technologies in which final pieces are created by the addition of smaller units of raw material, and oftentimes AM is simply used as a synonym of Rapid Prototyping (RP) or more informally of "3-D printing" regardless of the particular technology used to create the final assembly. The term AM is used in contrast to the traditional Subtractive Manufacturing (SM) technologies based on eliminating portions from a block of raw material to obtain the final part, usually employing techniques such as handcrafting, molding, and Computer Numerical Control (CNC) machining.

Among the most promoted advantages of AM over traditional alternatives [4, 5] stand out its lower prototyping cost and shorter developing time, due to the ability to build complex shapes in fewer iterations and almost entirely in the digital domain, mostly thanks to its seamless integration with Computer Assisted Design (CAD) software, what allows numerical validation and optimization before physical testing and therefore a quick transition from design to production.

Additive manufacturing of metals [6–8] is of special interest in industrial applications and has been successfully used in dental and bio-medical prosthesis, as well as in the production of components for aero-spatial and vehicular sectors. Interestingly in the case of AM of metal parts, money savings in the production of small to medium batches are expected [5, 9], as the flexibility in design, customization,

Received 18 July 2019, Accepted 14 October 2019, Scheduled 5 October 2019
* Corresponding author: Germán Augusto Ramírez Arroyave (garamirezar@unal.edu.co).
The authors are with the Universidad Nacional de Colombia, Colombia.

and re-design, allows building and testing optimized complex shaped parts and assemblies, reducing tooling time, costs and limitations.

In spite of all these advantages, AM still has a long way to go, before becoming the industry standard for manufacturing, having inherent technological limitations related to resolution: minimum wall thickness, and vertical step; with the consequent tolerances and roughness of the surfaces that can be achieved, often requiring post-processing to attain the desired finishing.

Specifically, in the case of metallic parts, the costs associated with equipment are still very high and directly translate into production costs, which is why building only one or a few units of a sample product may not be affordable in most cases. Moreover, practical combinations of scale, material, geometrical complexity, and cost are difficult to achieve with current technology (e.g., direct metal manufacturing in millimeter scales).

For these reasons, in some prototyping cases for industries where electrical in lieu of mechanical properties of metals are required, an appealing option is the metallization of pieces made by AM of plastic materials. This approach has shown very good results in antenna engineering and is opening new perspectives to designs that were unimaginable or only theoretically possible some years ago. In this regard, remarkable advances on 3-D-printed antennas have been developed in recent years, as a brief list of milestones: [10, 11] present horn antennas built via Stereolithography (SLA) with copper plating over a conductive silver ink coating; [12] introduces the manufacturing of compact antennas by means of conformal printing with conductive ink over 3D substrates; [13] presents application of titanium and subsequent copper cladding by vacuum sputtering in a variety of patch antennas realized by SLA.

Additionally, industrialization of AM techniques for antenna construction is at the basis of successful examples as [14] where two antennas for "Ku" band were designed and built in collaboration with a specialized company, the line of 3D printed antennas from [15], and [16] where industry partners joined efforts to validate manufacturing accuracy and repeatability of Selective Laser Melting (SLM) for horn antennas.

Although some of the mentioned examples are based on traditional antennas, which can be realized employing diverse construction methods, those constitute the steps validating the viability of AM for antenna manufacturing before going further to explore new geometries, possible only by the additional degrees of freedom provided by 3D structures, that can be directed to a better use of available space.

Performance bounds of Electrically Small Antennas (ESA) [17] were established in [18, 19], further reviewed by [20], and extended to general geometries among others in [21]. These results roughly state that ESA are subject to fundamental limitations of bandwidth, efficiency, and impedance matching, which complicate the simultaneous achievement of specific design goals such as multi-band/wideband behavior, gain, and compactness.

Notwithstanding that the antennas having a closer approximation to the theoretical limit are spherical and cylindrical helices and that AM has been successfully used for building that kind of structures [22], for practical reasons, compact antennas within portable devices [23] are customarily based on planar, 2.5-D and conformal structures employed due to their relatively simpler fabrication through techniques such as Printed Circuit Board (PCB) trace, Stamped metal, Flex-film, Hot-stamp, 3-D masking or Laser etching.

Without ignoring some ingenious 3-D designs that tackle the need for compactness such as the 3-D meander lines, variations of folded dipoles/monopoles, and Planar Inverted F Antennas (PIFA) with their variations such as the multi-layer PIFA [24], it can be said that traditional design approaches face serious limitations to perform impedance matching at multiple bands, mostly due to the presence of closely spaced metal parts with a high mutual coupling, causing that the smallest variation of parameters modifies the location of the antenna resonances, which sometimes act in interdependent manner [25, 26].

Optimization tools have demonstrated promising results supporting the assisted design of advanced function and compact antennas. For example [27–30] have shown compact low profile, PIFA like, and planar reconfigurable antennas that achieve a dynamic bandwidth in excess of 50%. The work herein presented elaborates on these efforts aiming to miniaturize the resulting antenna even further and leverage previous knowledge for the design of compact 3-D shapes.

With this aim, a 3-D template for optimization is proposed allowing, for example, the generation of radiators resembling a multilevel PIFA [31], with vertical connections among strata, thus accomplishing longer and diverse current paths while increasing the total antenna volume. This is expected to be

reflected in multi-band behavior and a compact volume, and additionally, realized antenna shapes suitable for AM, allowing an almost direct transition from Full-Wave Electromagnetic (FWEM) simulation to 3-D printing.

Inasmuch as this contribution is focused on one validation case for the proposed 3-D design and manufacturing methodology, its features are briefly stated. The objective is to design a dual-band antenna operating at 2.45 and 5.8 GHz, with dimensions $12 \times 12 \times 7$ mm or $0.098\lambda \times 0.098\lambda \times 0.057\lambda$ at the lower band, mounted at the center of a 40×40 mm ground plane with the consequent advantage that its radiation pattern shape is mostly oriented towards the antenna hemisphere, thus reducing the power radiated in unintended directions, and also that the impedance match does not degrade catastrophically when a placement offset is required as happens when traditional PIFA like antennas are moved away from the borders of the ground plane [32, 33].

Similar 3-D structures are presented in [34, 35], where a compact 3D cube is proposed for multi-band 4G operation using multi-band matching networks to enable ground plane radiation. This approach, however, is highly dependent on ground plane size and shape.

Similar performing antennas can be found for example in [36] where the same bands of operation are achieved with a PIFA enclosed in a volume of $23 \times 10 \times 5$ mm, placed on the edge of a ground plane with size 45×85 mm. A 3-D single band PIFA with similar electrical dimensions is presented in [37] with footprint dimensions of $0.209\lambda \times 0.126\lambda$. More recently, an optimized dual-band PIFA enclosed within a volume of $18.5 \times 8.5 \times 4$ mm operating around 3.5 and 5.6 GHz has been proposed as Antenna Element (AE) for Multiple-Input Multiple-Output (MIMO) operation in mobile phones [38]. In comparison to the aforementioned antennas, the reduced footprint and required ground plane size of our design makes it an appealing alternative for constrained space requirements.

Another kind of compact dual-band antennas is the low profile monopole presented in [39], whose lower band is 0.76 GHz in addition to the desired feature of frequency tunability, which achieves this with a 0.02λ height at the expense of a large ($0.246\lambda \times 0.246\lambda$) footprint, showing an implicit design trade-off of compact antennas that is tackled with our design.

An interesting compact PIFA-like antenna is presented in [40]. Although its dimensions are impressive, this antenna cannot be strictly considered a PIFA as the ground plane disposition and consequently its radiation pattern more resemble that of a monopole. Also, its first band presents a very poor match that can be degraded with changes in its surrounding environment.

Another alternative kind of compact antennas is those based on monopoles. For example [41] shows a tri-band plus Ultra Wide Band (UWB) antenna with a footprint of 30×30 mm and a lower match at 1.78 GHz, and likewise the compact designs of [42, 43] achieve good match at 500 MHz with a footprint of 15×15 mm. Nevertheless, these designs are prone to degradation of its radiation characteristics when being placed in the proximity of perturbing objects. Another approach to achieve impedance match at very low frequencies is to use a matching load as in [44]; however, it suffers from a low efficiency which limits its application in mobile communication systems.

On the side of antennas using similar manufacturing procedures, there are some recent works such as [45] where a 3-D single-band antenna based on a modified microstrip patch antenna, intended to use third dimension features as a means to achieve footprint compactness is introduced, and the overall dimensions of the realized prototype are about $0.326\lambda \times 0.275\lambda$, which make it at least three times larger than our proposal.

Also, [46] presents a large surface dual-band reflector made by Selective Laser Sintering (SLS) based on Nylon, and metallization is realized by silver ink coating. However, this approach is limited by ink conductivity, which besides being an expensive supply can degrade antenna efficiency. On the other hand, [47] shows another use of AM in developing a UWB antenna. An interesting approach to metallization is carried out by sputtering which creates a thin copper (Cu) layer followed by electroplating to achieve a thick Cu layer. Similar to our work, the proposed complex antenna shape requires that the modules are printed and metallized in a separate fashion and joined in a final step.

In summary, this paper presents an extension to 3-D structures of an efficient Genetic Algorithm (GA)-MoM assisted electromagnetic design technique that considers, in the design, the topology of the template and the enabling possibilities of its outcomes as well as its manufacturability by AM technology, resulting in a very compact prototype that could be realized with very low-cost techniques achieving results very close to the design.

Indeed, further benefits can be achieved when more stringent optimization goals are pursued, such as beam-steering, multi-port operation, frequency reconfigurability, or a combination of those objectives. Therefore, it is expected that present and upcoming advances in additive (3-D) manufacturing will motivate the application of design methodologies such as the one presented here to exploit the known potential of 3-D radiating structures.

The remainder of this paper is organized as follows: Section 2 presents the initial structure used in the optimization stage, which is described in Section 3. Then, full-wave simulation results are presented in Section 4 as proof of concept, including a comparison of performance in different settings of ground plane size, construction material, and metal thickness variation. Afterwards, a scaled antenna prototype is presented in Section 5 as validation. Finally, Section 6 presents the main conclusions and recommendations regarding the future use of this kind of antennas.

2. PIXEL ANTENNA TEMPLATE

The initial structure, from which optimum antenna is derived, is made of planar metal surfaces only and is composed of three portions as shown in Fig. 1: a rectangular hexahedron located on top and constituted by a $7 \times 7 \times 3$ grid of interlocking coordinate surfaces orthogonal to the respective Cartesian axes (the solid black lines show cuts of these plane segments), forming pixels of $a = 2\,\text{mm} \times a = 2\,\text{mm}$; 24 grounding straps with height $b = 3\,\text{mm}$ emerging from the bottom perimeter of the former; and a ground plane with size $l = 40\,\text{mm} \times l = 40\,\text{mm}$.

During the design process, the pixels in the hexahedron (only the outer front ones visible in Fig. 1) and the straps will be removed selectively, to optimize electrical performance (geometry optimization), while the ground plane remains fixed. Another degree of freedom is the port location, which may be chosen among any one of the grounding straps present (hence the straps present are either an input port or an actual shorting strap). Note that in the design stage, all the metal is assumed to be Perfect Electric Conductor (PEC) with negligible thickness.

The volume occupied by the optimizable part of the antenna is just 1cm^3 or in terms of wavelength $0.098\lambda \times 0.098\lambda \times 0.057\lambda$ at the minimum operating frequency. The total number of binary variables required to represent each possible geometrical setup is 300 (276 square plates for the hexahedron plus 24 straps to ground). Note that these bits simply state the presence or not of a metal feature and do not by themselves define the feeding port location; hence, a given bit string (i.e., "chromosome") actually defines k structures with identical geometry, yet different port locations across its k shorting straps. The selection among these structures is made implicitly during optimization by selecting the best performing variation.

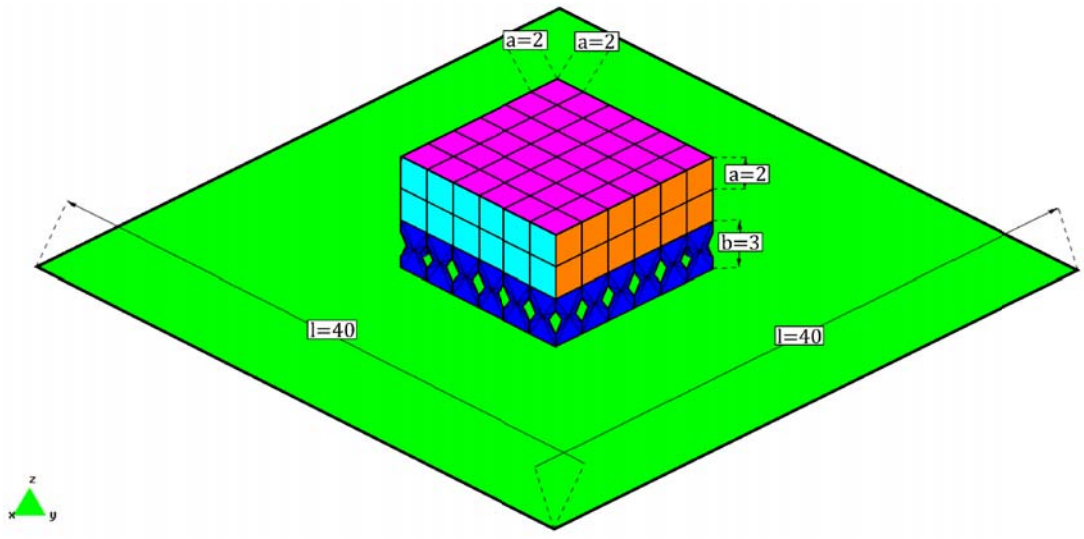

Figure 1. Initial structure for the antenna (dimensions are in mm).

The initial structure was conceived to allow structured 3-D geometries that can be coded and manufactured with relative ease. The template proposed allows for example the generation of radiators resembling a multilevel PIFA with vertical connections among strata, thus allowing longer and diverse current paths while increasing the total antenna volume. This is expected to be reflected in multi-band behavior and a compact volume, as many of the following downsizing techniques [48] could be approximated by a suitable pruning of the template: Multi-layered (fold, bend, stack), Patch etching (slits, slots, notches), Shorting Planes (walls, pins).

One salient feature of the proposed design approach is the manufacturability of the realized antenna shapes, as the optimization template is intended to achieve structures that can be monolithically built by AM. However, the manufacturing process might not be straightforward given some technological limitations, e.g., relying on horizontal walls printed with the use of soluble supporting material can be problematic for Fused Deposition Molding (FDM) and SLA technologies. Accordingly, another advantage of the resulting structures can be exploited, namely its modularity which allows for printing the individual "floors" of the antenna and then joining them. It is worth mentioning that in this work the manufacturing approach consists of mixing AM based on FDM of plastic materials with a subsequent surface metallization.

3. OPTIMIZATION PROCESS

The basics of the optimization procedure, which is based on full-wave MoM simulation and GA optimization, are thoroughly covered in [27]. The first step consists of the simulation of an initial template structure which is a kind of power-set of all the candidate solutions to be analyzed during the optimization process; this happens since the candidate solutions result from material subtraction from the template. The MoM interaction matrix $\mathbf{Z}$ is computed for the (full) template structure; then, in the GA optimization phase, the performance of each individual is evaluated with a reduced $\mathbf{Z}$ matrix in which the rows and columns related to removed metal ("off" bits in the individual's chromosome) are not present. It should be remarked that using this procedure, each candidate solution is evaluated using full-wave simulation in a very efficient way, instead of being replaced by a surrogate model to obtain an estimate of its performance.

With respect to [27, 28], the 3-D structures considered here present the possibility of junctions of three or four facets; for simplicity in the generation of the possible topologies resulting from pruning the original junctions, the full $\mathbf{Z}$ matrix includes the Rao-Wilton-Glisson (RWG) functions composed of every facet pair ($n(n-1)/2$ for a junction with n facets), which results in a redundant representation for the current that would produce an ill-conditioned reduced $\mathbf{Z}$ matrix. For this reason, at every step during optimization it is ensured that junctions of n facets have exactly $n-1$ RWG functions defined on each of them by randomly eliminating rows/columns of the $\mathbf{Z}$ matrix associated with functions in excess of the minimum required. A further addition was to allow optimization of input port locations, which are selected among the straps present; indeed, for a candidate design with n straps present and m input ports desired (e.g., as in duplexing/diversity/MIMO applications), the optimizer tests each of the $\binom{m}{n}$ possible choices, selecting the one with the best performance, which is possible thanks to our highly efficient full-wave computation. The straps other than the input ports could be connected to ground via arbitrary impedances (e.g., as switches in reconfigurable designs); however, in the present work we demonstrate the case of a design with one input port and shorting straps, so the resulting design is "static" (i.e., non-reconfigurable).

In addition to the aforementioned modifications, a structural validation of individuals is done in order to ensure the correctness of the electromagnetic solution given by the reduced MoM matrix, which also leads to antennas simpler to manufacture. This validation consists in ensuring that there are no metal portions connected only by a vertex. Given the 3-D template structure, there are $2^{12} = 4096$ possible metal configurations at each vertex (each vertex touches twelve metal squares), so the geometrical verification and correction needs to be made in an efficient manner in order to reduce impact on the total computation time.

Despite the automatic input port selection, strap location search, and exhaustive vertex validation and correction process, the complete optimization process took less than five hours in a portable computer with an Intel core i7 processor, 8 GB of RAM, and no GPU acceleration nor parallel GA

computing.

3.1. Optimization Parameters

Table 1 summarizes values of the parameters used in the GA run.

Table 1. Parameters for the optimization process.

Parameter	Value
Chromosome length (bits)	300
Population size (individuals per generation)	1000
Number of generations	300
Maximum number of straps allowed	4
Target reflection coefficient $\|S_{11}\|_{\mathrm{dB}}$	-15

For the dual-band optimization at hand, the cost function includes the worst (maximum) reflection coefficient $|S_{11}|_{\mathrm{dB}}$ among the specified frequency samples of 2.45 GHz and 5.8 GHz and the number of straps; when these conform to the limits specified in Table 1, optimization is stopped. No bandwidth requirement is imposed at the established frequencies.

Given the complexity of the problem, a large number of generations were anticipated; however, the GA converged to the desired minimum in just 107 generations. It is worth mentioning that the process required over one hundred thousand full-wave simulations, with exhaustive search of port location at each of these, which highlights the efficiency of the process.

3.2. Optimized Structure

After examining the results of various optimization runs, the second best individual of one population converging to optimum was chosen. This choice is supported on the higher robustness of this realization to manufacturing tolerances, particularly smaller changes of impedance match, and resonant frequencies with variations of metal thickness, which were evidenced during the full-wave validation.

The reflection coefficient of the chosen structure, as predicted by the optimizer, was $S_{11} = \{-18.4388\,\mathrm{dB}, -14.1730\,\mathrm{dB}\}$ at the two frequency samples considered. As the antenna is only composed by metal and is modeled by PEC, the predicted efficiency is 100%. The S_{11} values will in general present some offset with respect to more accurate full-wave simulations as the meshing used for optimization is not adaptive, and no edge refinement is done. Furthermore, with the frequency sampling and optimization target chosen, it cannot be implied that the resulting resonance frequencies are located at the samples, nor that the minimum reflection coefficient is located there. Similarly, nothing prevents the presence of additional resonance frequencies in the intervening bands. These aspects were not deemed a serious concern in our application, so we maintained the simplest problem specification that provided useful optimization results; however, these and similar considerations could be taken into account should the application require it by a suitable modification of the sampling and cost function, with the corresponding increase in computational burden.

Some views of the optimized antenna can be seen in Figure 2. Although it is hard to appreciate the complete 3-D structure, the 4 views presented aid in inferring the optimized antenna shape. It can be seen that the antenna has three straps besides the feeding port, which is plotted with a gap.

Similar to what is usual with the conventional PIFA, straps concentration on one side of the antenna may make it seem unstable at first sight, but thanks to its lightweight manufacturing, the antenna stands firmly without additional support. Nevertheless, one could also include restrictions such as straps on opposite sides of the structure in order to achieve improved structural stability of the final design, by a suitable modification of the cost function.

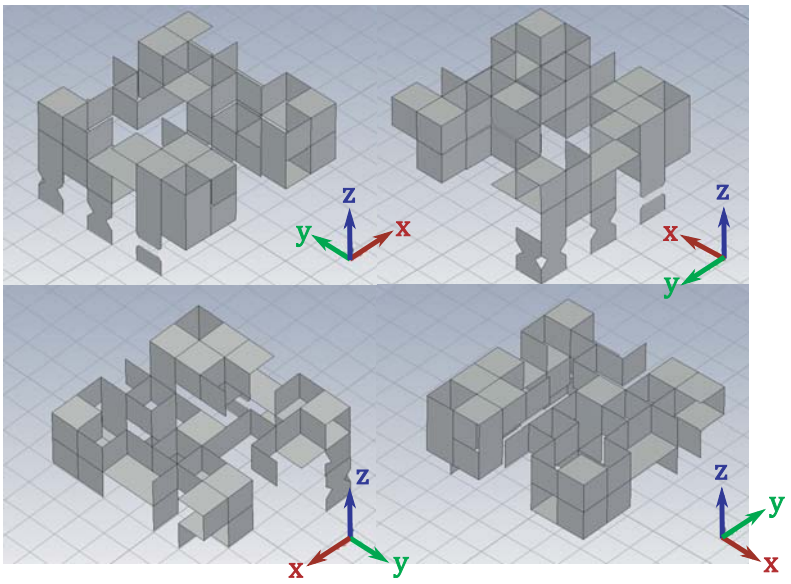

Figure 2. Views of the optimized 3D antenna.

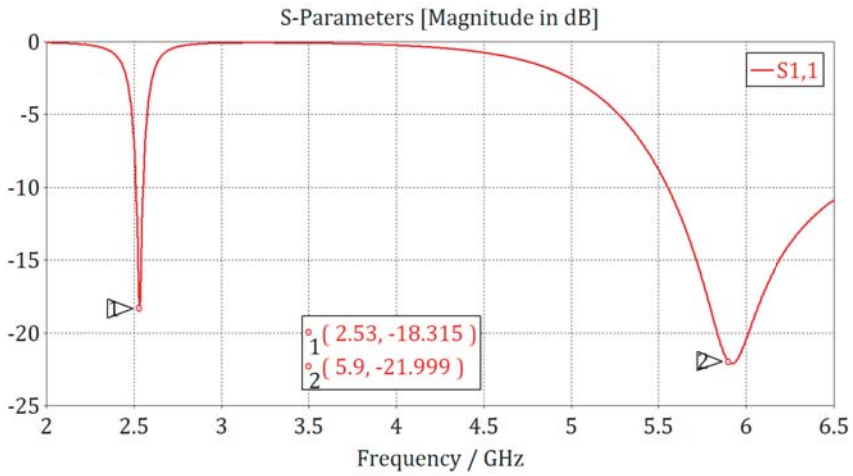

Figure 3. Reflection coefficient of the optimum antenna computed with CST.

4. FULL WAVE VALIDATION

After performing the structure optimization, we initially validated the antenna structure through re-simulation with our MoM software using a finer mesh generated from scratch. In addition, a cross validation is carried out by using the integral solver in CST studio, which is deemed appropriate given the intricate geometry and the narrow-band behavior expected. The reflection coefficient can be seen in Figure 3. It is observed therein that the two bands predicted by the optimizer are present with minima in $f = 2.53\,\text{GHz}$ and $f = 5.9\,\text{GHz}$. At the lower frequency, given the narrow-band behavior, the result amounts to a deviation of 3.2% with respect to 2.45 GHz, while in the upper frequency the performance conforms to the optimization result.

There can also be seen that the $-10\,\text{dB}$ reflection coefficient bandwidth is about 1.7% and 20% in the low and high frequencies, respectively. This narrow band behavior in the low frequency band is expected due to the reduced electric volume of the structure at that frequency, which results in a high Q value.

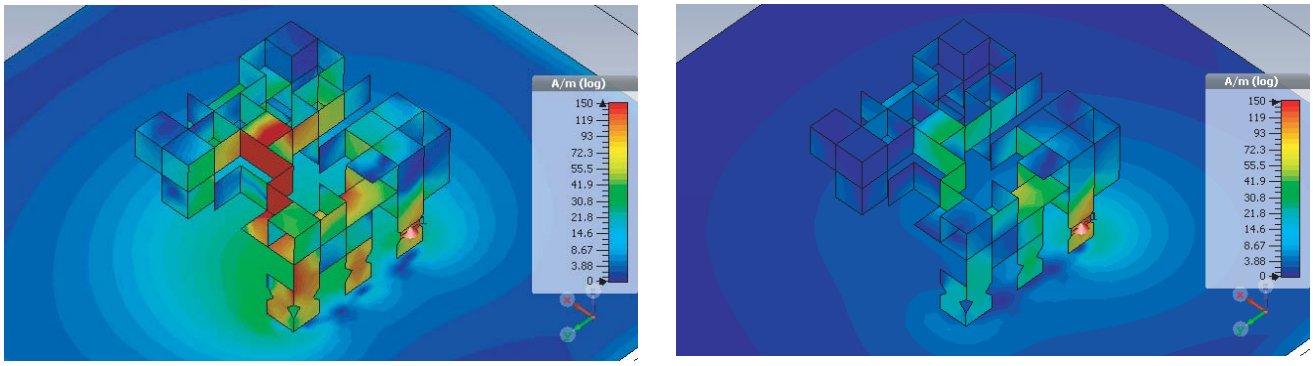

(a) (b)

Figure 4. Surface currents on the antenna. (a) Low band. (b) High band.

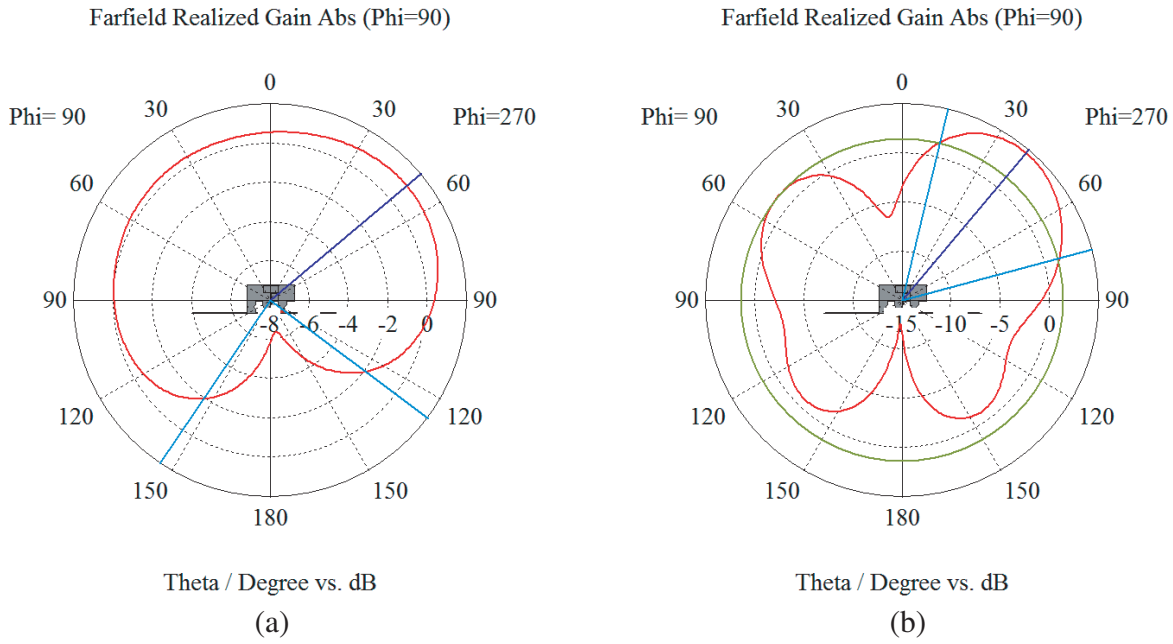

(a) (b)

Figure 5. Simulated realized gain. (a) Low band. (b) High band.

Current distributions on the antenna were also simulated at the matching frequencies of $f = 2.53$ and $f = 5.9$ GHz, proving that there are two main paths across the structure which are responsible for radiation, as can be seen in Figure 4. In the low band, an important portion of the antenna including its grounding straps is strongly excited, whilst in the high band current intensity is lower, and a minor antenna portion is active. It can also be appreciated that the ground plane is not significantly excited at any of the two bands and hence has a small contribution to radiation. This is corroborated with additional simulation runs varying the ground plane size to $\{30 \times 30,\ 18 \times 18\}$ mm, achieving minima of frequency match at $(f_1, f_2) = \{(2.56, 5.95), (2.69, 6.25)$ GHz, with similar bandwidth characteristics.

As an additional result, it can be seen in Figure 5 that radiation occurs predominantly towards the top hemisphere, which is expected from the presence of the ground plane. Such a behavior may prove beneficial in terms of reduced power loss, reduced SAR in setups where the antenna is to be placed near the human body, and reduced interference with components in the opposite side of the ground plane.

Likewise, it can be appreciated that the realized antenna gains in the inferior and superior bands are 1.064 and 4.533 dB, respectively, proving that the antenna is an efficient radiator in the lower frequency,

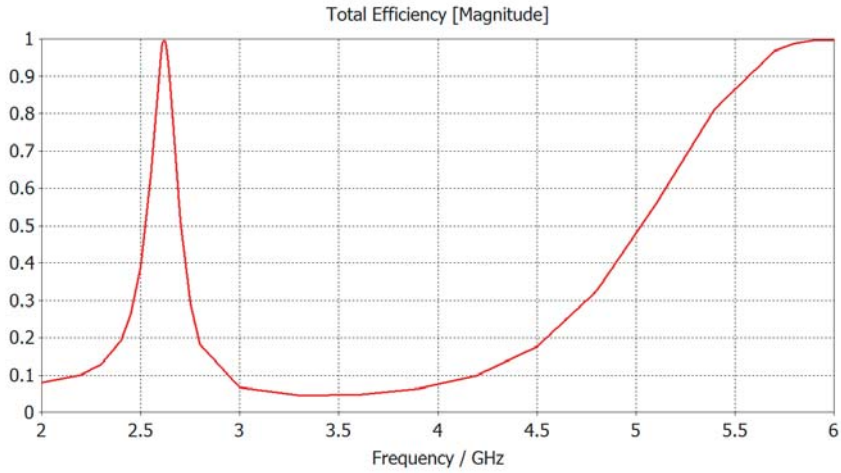

Figure 6. Antenna efficiency.

considering its electrical size and the physical limits established in [49].

To further demonstrate the radiating capabilities of the compact antenna, efficiency is simulated using a model reflecting the manufacture process consisting of a supporting structure made of Acrylonitrile Butadiene Styrene (ABS), $\epsilon_r = 2.74$, $\tan\delta = 0.025$ [50], with a thickness of 0.2 mm and a copper shell recreating the metallization cover. The total efficiency is illustrated in Fig. 6, where a 99.6% is predicted at both match frequencies, proving that the plastic material has a minor impact on the antenna performance.

4.1. Material Variation

As mentioned before, the initial MoM simulation and optimization is carried out considering the antenna made of PEC for the sake of efficiency, as previous experience showed that copper realizations should not severely degrade the antenna performance.

With the aim of forecasting the performance of a built antenna prototype, two common materials suited for additive manufacturing of antennas are compared to PEC, Aluminum (Al) and Copper (Cu). The former is the main component of many alloys commonly used in direct 3-D Direct Metal Laser Sintering (DMLS) and also can be deposited over a dielectric surface by means of sputtering, while the

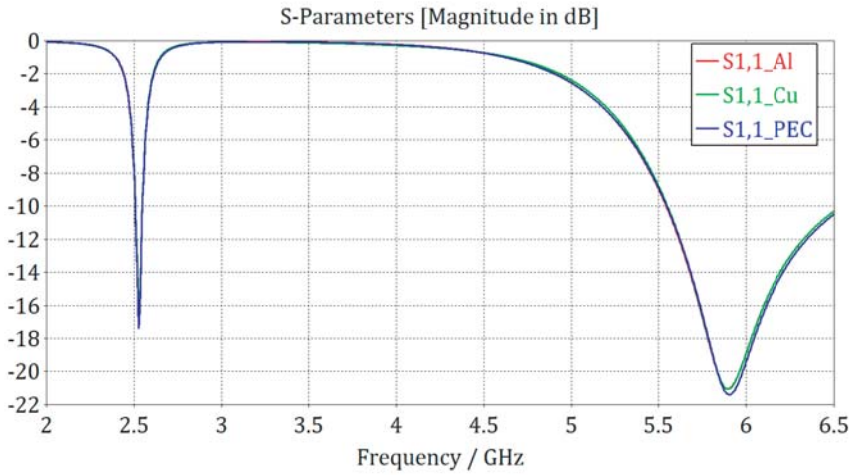

Figure 7. Variation of S_{11} with building material.

later can be used as a coating either by electroplating, electroless plating, or any other metallization techniques suitable for dielectric plastics.

Figure 7 presents the comparison of the S_{11} parameter for the three materials considered, and as can be seen there are not noticeable differences among them.

A further step into this direction was the simulation of a copper/aluminum metallic shell filled with ABS. This is a worst-case simulation recreating actual manufacturing, and as in the previously mentioned ones, no significant changes are noticed, which indicates that the proposed fabrication process does not degrade the antenna performance compared to a purely metallic prototype.

4.2. Performance Variation with Metal Thickness

Taking into account that the MoM formulation used is surface-based and that the cube pixellation is also based on square facets, optimization results are valid to the extent that a sheet approximation of the resulting individual pixels still holds.

However, looking forward for a 3-D printing realization of this antenna, a test was performed to estimate the antenna behavior against metal thickness (th) variations, showing that the effect of changing this parameter has a minor impact on the antenna's matching behavior as can be appreciated

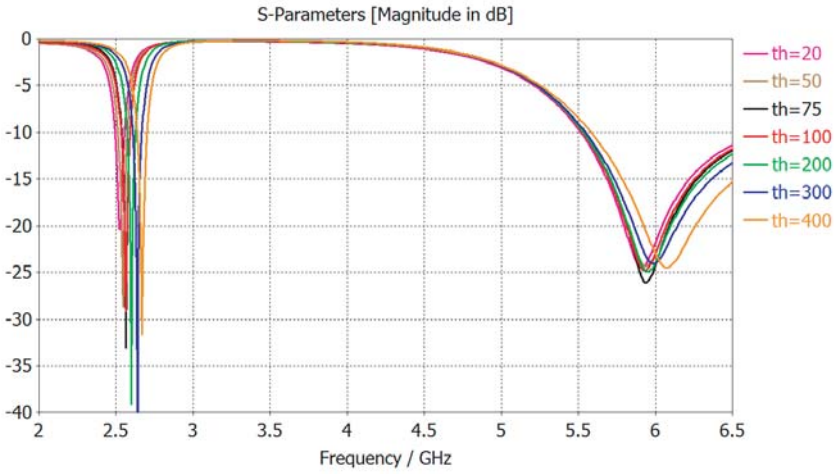

Figure 8. Variation of S_{11} with metal thickness 'th', in μm.

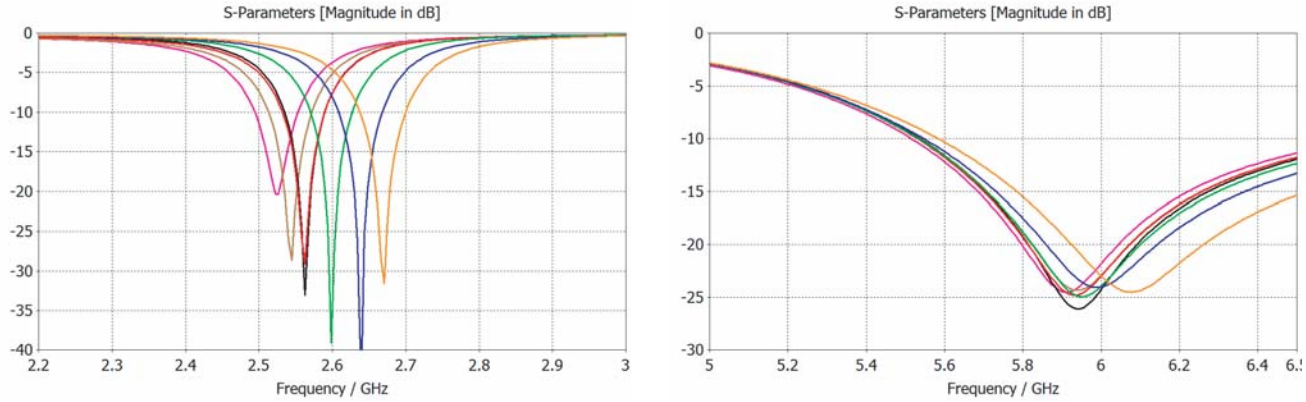

Figure 9. Detail of S_{11} variation with metal thickness at the matching bands. (a) Lower band. (b) Higher band.

in Figure 8. It can be seen that the laminar approximation is enough for metal thickness under 0.1 mm, as frequency deviation is 1% from that predicted for sheet pixels.

Taking a closer look, in Figure 9 it can be appreciated that in the lower band the match frequency increases as the metal thickness does, which can be partly attributed to the inductive nature of the input impedance, despite that nearby plates are found throughout the antenna. It can also be seen that in the higher band the variations with metal thickness are less pronounced.

5. ANTENNA PROTOTYPE MANUFACTURING

Fabrication of a three times $(3:1)$ scaled-up prototype of the antenna was pursued to demonstrate that this kind of complex shape antennas can be realized with very low cost procedures, based on standard FDM 3-D printing of ABS plastic material, taking into account the practical limitations that establish minimum thickness of printed walls, as well as minimum overall structure size.

Due to the complex shape of the antenna and the inability of the FDM technology to support horizontal walls without the use of vertical supports, which cannot be easily removed later, the antenna was built using a floor by floor approach. As can be seen in Figure 10 two floors plus a set of four individual pixels (not shown in figure) were individually printed and then glued together to form the final antenna assembly.

The printing of the antenna was done using a Makerbot Replicator 2X, whose nozzle size is stated as 0.4 mm. Several runs using wall thickness of $\{0.4, 0.5, 0.6, 0.7, 0.8\}$ mm showed that there were some pixels skipped by the printer software when using $\{0.4, 0.5\}$ mm thicknesses. This technical limitation supported the decision of making the 3 times scaled up version of the antenna ($36 \times 36 \times 21$ mm) with 0.6 mm thick walls.

In our prototyping, metallization was carried out by two different techniques: a) Electroplating to create a copper cladding. b) Vacuum metal deposition to create an aluminum cladding. A summary of the technologies considered for building the prototype is presented in Table 2. Further details about

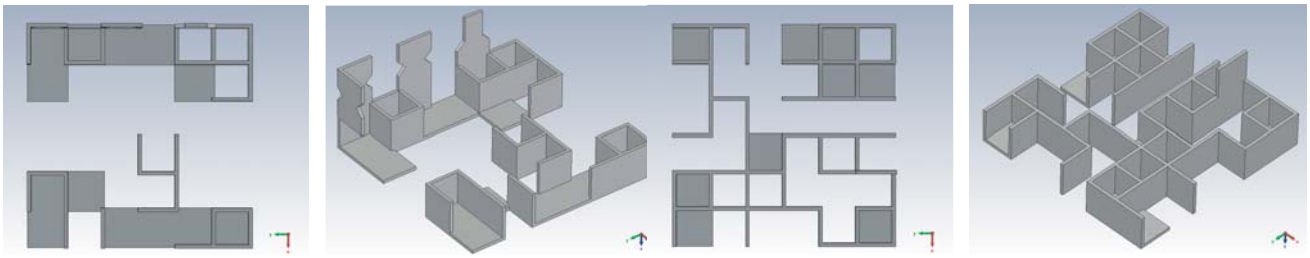

(a) (b) (c) (d)

Figure 10. Antenna 'floors' for 3D printing. (a) 1st floor top view. (b) 1st floor. (c) 2nd floor top view. (d) 2nd floor.

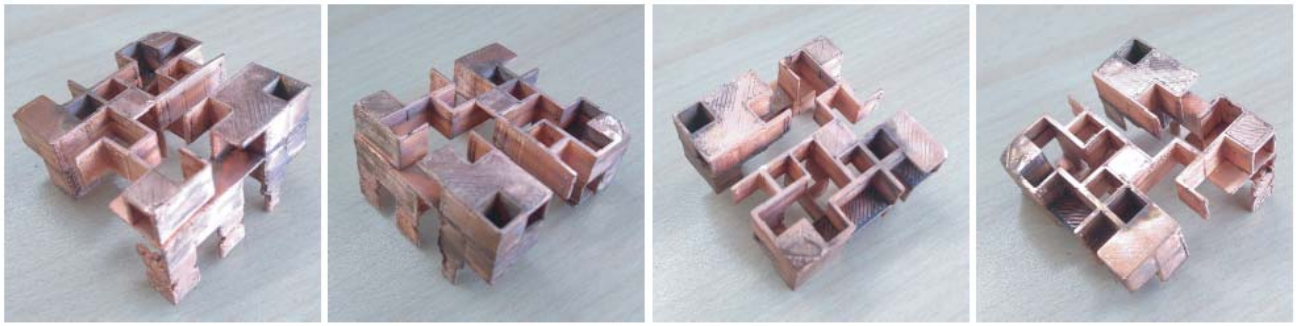

Figure 11. Manufactured 3D antenna with copper cladding.

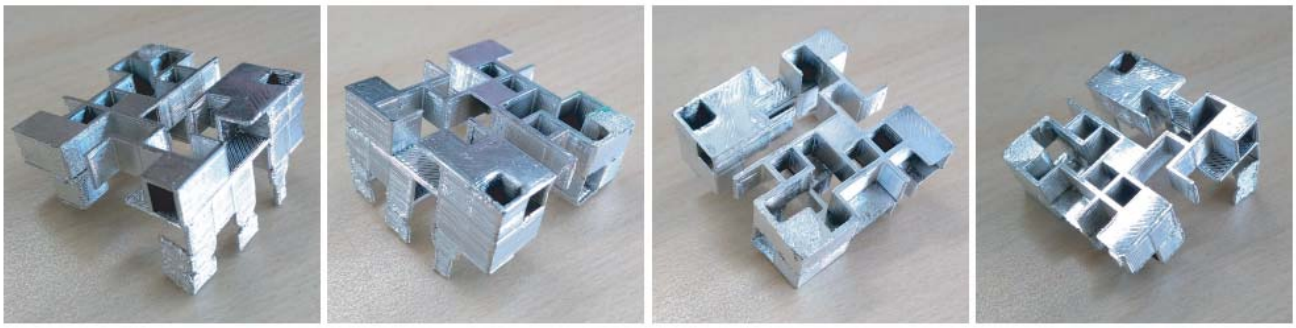

Figure 12. Manufactured 3D antenna with aluminum cladding.

Table 2. Comparison of manufacturing technologies considered.

Technology	Description	Advantages	Disadvantages
Tooling	Metal cutting and bending in a workshop	• Easy. • Very low cost.	• Not appropriate for the geometry under consideration.
DMLS	Direct Metal Laser Sintering (Based on metal powder)	• Broad range of materials (availability of high conductivity Aluminum alloys). • Does not require further processing. • Monolithic construction of complex shapes.	• Very expensive. • Small scales are hard to achieve.
SLA	Stereolithography (UV curing of polymer)	• Very small scales can be achieved. • Supports different kinds of metallization.	• Costly. • Shape limitations (truly 3-D requires supporting structures that needs to be later removed).
FDM	Fused Deposition Molding (Plastic extruded and layered)	• Low cost of ownership. • Well suited for metallization (Electroplating/Vacuum Metal Deposition). • Separate pieces can be assembled using epoxy adhesive. • Soluble filaments as supporting material,	• Complex shapes can not be made in monolithic fashion.

the performance of these techniques for the AM of antennas can be consulted in [51].

Once the floors are printed and assembled, and the metallization procedures are carried out, two final antenna prototypes are achieved as can be appreciated in Figures 11 and 12.

The first one, electroplated copper, has proven more resistant to scratching, thermal and mechanical

stress, even allowing the antenna to be soldered to the ground plane, while the second one, sputtered aluminum, showed a poorer mechanical and thermal resistance, being easily removed by scratching and impossible to solder, hence connection had to be made by contact pressure.

A real size (1 : 1) antenna prototype was also manufactured by using SLA 3-D printing with satisfactory results. In this case similar procedures to those employed for the FDM prototype printing by floors and later assembly were used. Metallization alternatives for this version are currently a subject of study.

5.1. Measurements

In order to make reliable measurements of the antenna parameters, a mechanism for mounting the antenna to the ground plane must be implemented. In the copper cladded case, the antenna could be attached to the ground plane by conventional soldering, taking care of keeping time and temperature as low as possible, whereas in the aluminum case, it was necessary to create a support structure soldered to the ground plane to hold the antenna as tight as possible; another alternative in this case could be the use of conductive (silver), but this was not tested.

The details of the mounted antennas and support can be appreciated in Figure 13.

Figure 13. Antenna mounting on 150 × 150 mm ground plane.

With the aid of this setup, S_{11} parameters of the manufactured scaled-up antennas were measured and compared against a re-simulation of the antenna; results can be seen in Figure 14.

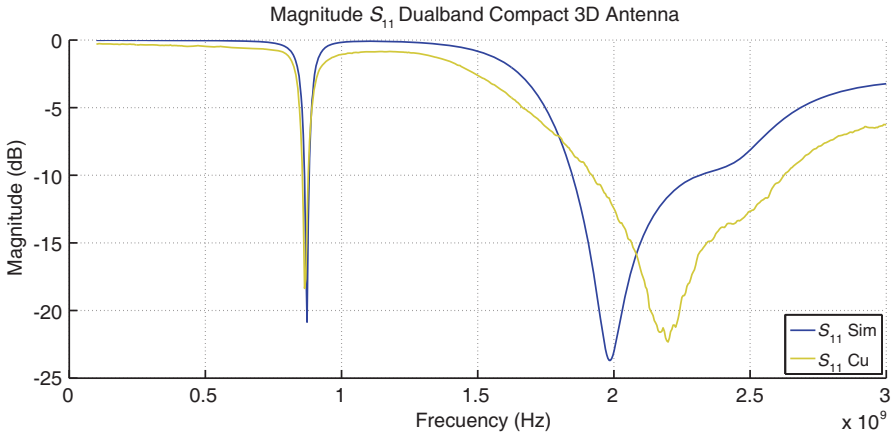

Figure 14. Measured reflection coefficient of the 3 : 1 antenna prototype.

It can be appreciated that the copper prototype presents a very good agreement with simulated data concerning dual-band behavior and the best matching values. We do not report results for the

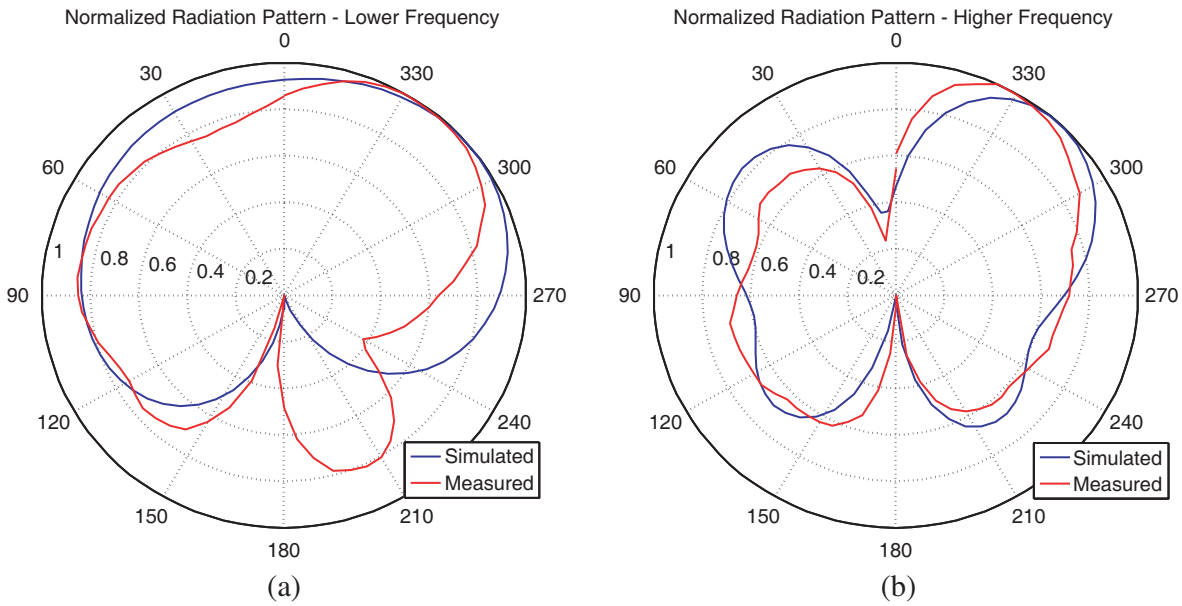

Figure 15. Radiation pattern of the realized antenna. (a) Low band. (b) High band.

aluminum version of the antenna as these were indicative of problems with the mechanical attachment employed and the conductivity of the coating.

Radiated fields of the antenna prototype were also measured at both match frequencies. Maximum realized gains of 1.3 and 3.94 dB are observed at the lower and higher bands, respectively, and those values are in good agreement with the 1.13 and 3.61 dB predicted in re-simulation. Normalized pattern plots are presented for the copper version in Figure 15. A very good correspondence between simulation and measurement can be observed, confirming the reliability of the design and manufacturing processes presented.

Table 3. Comparison to other antennas reported in literature.

Reference	Antenna kind	(Minimum) Operation frequency (GHz)	Bandwidth (%)	Minimum enclosing sphere diameter	Ground plane size (mm)	Gain (dBi)	Efficiency (%)
This paper	3D pixel patch	2.45 & 5.8	1.7 & 22	$0.15\lambda_0$	40×40	1.3 & 4.5	99.6 & 99.6
[36]	PIFA	2.45 & 5.8	7 & 32	$0.21\lambda_0$ mm	45×85	1.98 & 3.82	NR
[37]	PIFA	1.575	2.5	$0.21\lambda_0$	NR	2.8	NR
[38]	PIFA	3.5 & 5.6	13 & 24	$0.24\lambda_0$	55×110	NR	90 & 97
[39]	Low profile monopole	0.9 & 1.75	4 & 7	$0.375\lambda_0$	280×280	2 & 5.5	100
[40]	Monopole/ PIFA	0.89 & 1.95	15 & 25	$0.096\lambda_0$	55×90	NR	NR
[41]	Monopole	1.78	3	$0.25\lambda_0$	30×9.6	-3.5	NR
[44]	Monopole	0.5	144	$0.035\lambda_0$	15×3.8	0.1	15
[42]	Monopole	1.59 & 3.82 & 5.71	137 & 32.5 & 31.2	$0.132\lambda_0$	NA	1.6 & 3.7 & 4	41 & 78 & 83
[43]	Loaded patch	0.48	172.5	$0.033\lambda_0$	17×23	0.4	8

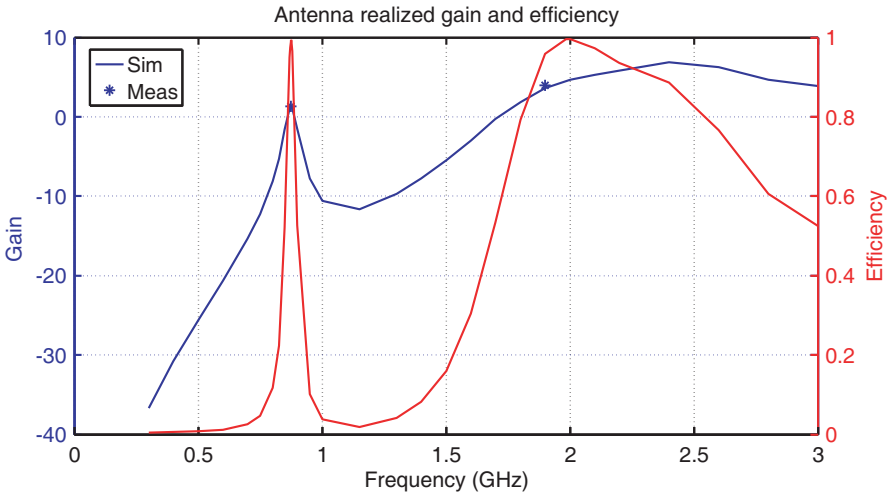

Figure 16. Gain and efficiency of the 3 : 1 scaled antenna prototype.

Likewise, Fig. 16 presents the gain and efficiency of the scaled prototype, and a very good agreement of measured gains at the sampled frequencies is found.

As a final remark, Table 3 summarizes the main results of the miniature 3-D pixel antenna, compared to conventional compact antennas reported in literature in terms of frequency, bandwidth, size, gain, and efficiency. For PIFA and PIFA-like designs, the minimum enclosing sphere considers only the radiator part disregarding the contribution of the ground plane to particular designs. The proposed design has similar performance to other PIFA like antennas in a more compact volume with a smaller ground plane requirement.

6. CONCLUSIONS

This contribution has presented the full workflow for an ultra-compact volumetric pixel patch antenna that can be considered as an evolution of the multilevel PIFA, with a 33% reduction in the footprint. The resulting design displayed robust performance against manufacture parameters such as metal conductivity and thickness, and ultimately robustness against manufacture tolerances, as the measured performance matches very well that expected from simulation.

The techniques used for adding a metal finishing to the presented antenna have proven useful. However, copper cladding had some advantages inherent to the electroplating process compared to the vacuum deposition of aluminum, such as good deliver in harder to reach parts of the antenna. This process also presents other advantages related to its mechanical and thermal resistance, which make the antenna integration easier to other system components. It should be noted that the prototype made with aluminum displayed a behavior that indicates problems with the mechanical connection mechanism required and the metal loss of the coating.

The combination of these results with our previous experience in the design of multi-port reconfigurable antennas allows us to envision further ultra-compact 3-D designs with extended functionality, as the optimization technique is fully general and can simultaneously consider electromagnetic, geometric, structural, cost, and other design goals.

ACKNOWLEDGMENT

This work was partly funded by COLCIENCIAS grant "Convocatoria 727 — doctorados nacionales" and by Universidad Nacional de Colombia, División de Investigación y Extensión Sede Bogotá — DIEB. Plastinnova and Servicrom have provided the metallization services. Radiation patterns were measured at the anechoic chamber of the Universidad de los Andes in Bogotá. The Grupo de Trabajo en Nuevas

Tecnologías de Diseño Manufactura-Automatización DIMA-UN has collaborated in the manufacture of the '1 : 1' scale prototype.

REFERENCES

1. Gao, W., Y. Zhang, D. Ramanujan, K. Ramani, Y. Chen, C. B. Williams, C. C. Wang, Y. C. Shin, S. Zhang, and P. D. Zavattieri, "The status, challenges, and future of additive manufacturing in engineering," *Computer-Aided Design*, Vol. 69, 65–89, 2015, [online], available: http://www.sciencedirect.com/science/article/pii/S0010448515000469.
2. Tofail, S. A., E. P. Koumoulos, A. Bandyopadhyay, S. Bose, L. O'Donoghue, and C. Charitidis, "Additive manufacturing: Scientific and technological challenges, market uptake and opportunities," *Materials Today*, Vol. 21, No. 1, 22–37, 2018, [online], available: http://www.sciencedirect.com/science/article/pii/S1369702117301773.
3. Ituarte, I. F., E. Coatanea, M. Salmi, J. Tuomi, and J. Partanen, "Additive manufacturing in production: A study case applying technical requirements," *Physics Procedia*, Vol. 78, 357–366, 2015, *15th Nordic Laser Materials Processing Conference, Nolamp 15*, [online], available: http://www.sciencedirect.com/science/article/pii/S1875389215015400.
4. Gibson, I., B. Stucker, and D. Rosen, *Additive Manufacturing Technologies*, Springer-Verlag, New York, 2015.
5. Attaran, M., "The rise of 3-D printing: The advantages of additive manufacturing over traditional manufacturing," *Business Horizons*, Vol. 60, No. 5, 677–688, 2017, [online], available: http://www.sciencedirect.com/science/article/pii/S0007681317300897.
6. DebRoy, T., H. Wei, J. Zuback, T. Mukherjee, J. Elmer, J. Milewski, A. Beese, A. Wilson-Heid, A. De, and W. Zhang, "Additive manufacturing of metallic components — Process, structure and properties," *Progress in Materials Science*, Vol. 92, 112–224, 2018, [online], available: http://www.sciencedirect.com/science/article/pii/S0079642517301172.
7. Frazier, W. E., "Metal additive manufacturing: A review," *Journal of Materials Engineering and Performance*, Vol. 23, No. 6, 1917–1928, Jun. 2014, [online], available: https://doi.org/10.1007/s11665-014-0958-z.
8. Herzog, D., V. Seyda, E. Wycisk, and C. Emmelmann, "Additive manufacturing of metals," *Acta Materialia*, Vol. 117, 371–392, 2016, [online], available: http://www.sciencedirect.com/science/article/pii/S1359645416305158.
9. Atzeni, E. and A. Salmi, "Economics of additive manufacturing for end-usable metal parts," *The International Journal of Advanced Manufacturing Technology*, Vol. 62, No. 9, 1147–1155, Oct. 2012, [online], available: https://doi.org/10.1007/s00170-011-3878-1.
10. Huang, Y., X. Gong, S. Hajela, and W. J. Chappell, "Layer-by-layer stereolithography of three-dimensional antennas," *2005 IEEE Antennas and Propagation Society International Symposium*, Vol. 1A, 276–279, Jul. 2005.
11. Maas, J., B. Liu, S. Hajela, Y. Huang, X. Gong, and W. J. Chappell, "Laser-based layer-by-layer polymer stereolithography for high-frequency applications," *Proceedings of the IEEE*, Vol. 105, No. 4, 645–654, Apr. 2017.
12. Adams, J. J., E. B. Duoss, T. F. Malkowski, M. J. Motala, B. Y. Ahn, R. G. Nuzzo, J. T. Bernhard, and J. A. Lewis, "Conformal printing of electrically small antennas on three-dimensional surfaces," *Advanced Materials*, Vol. 23, No. 11, 1335–1340, 2011, [online], available: https://onlinelibrary.wiley.com/doi/abs/10.1002/adma.201003734.
13. Ghazali, M. I. M., E. Gutierrez, J. C. Myers, A. Kaur, B. Wright, and P. Chahal, "Affordable 3D printed microwave antennas," *2015 IEEE 65th Electronic Components and Technology Conference (ECTC)*, 240–246, May 2015.
14. Van der Vorst, M. and J. Gumpinger, "Applicability of 3D printing techniques for compact Ku-band medium/high-gain antennas," *2016 10th European Conference on Antennas and Propagation (EuCAP)*, 1–4, Apr. 2016.

15. Tech, O., "Metal 3D printed custom antennas," 2018, [online], available: https://www.optisys.tech/.
16. Foged, L. J., A. Giacomini, R. Morbidini, F. Saccardi, V. Schirosi, M. Boumans, B. Gerg, and D. Melachrinos, "Investigation of additive manufacturing for broadband choked horns at X/Ku band," *IEEE Antennas and Wireless Propagation Letters*, Vol. 17, No. 11, 2003–2007, Nov. 2018.
17. Hansen, R. C. and R. E. Collin, *Small Antenna Handbook*, Wiley-IEEE Press, 2012.
18. Wheeler, H. A., "Fundamental limitations of small antennas," *Proceedings of the IRE*, Vol. 35, No. 12, 1479–1484, Dec. 1947.
19. Chu, L. J., "Physical limitations of omni-directional antennas," *Journal of Applied Physics*, Vol. 19, No. 12, 1163–1175, 1948, [online], available: http://dx.doi.org/10.1063/1.1715038.
20. McLean, J. S., "A re-examination of the fundamental limits on the radiation Q of electrically small antennas," *IEEE Transactions on Antennas and Propagation*, Vol. 44, No. 5, 672, May 1996.
21. Yaghjian, A. D. and H. R. Stuart, "Lower bounds on the Q of electrically small dipole antennas," *IEEE Transactions on Antennas and Propagation*, Vol. 58, No. 10, 3114–3121, Oct. 2010.
22. Kim, O. S., "Rapid prototyping of electrically small spherical wire antennas," *IEEE Transactions on Antennas and Propagation*, Vol. 62, No. 7, 3839–3842, Jul. 2014.
23. Rowell, C. and E. Y. Lam, "Mobile-phone antenna design," *IEEE Antennas and Propagation Magazine*, Vol. 54, No. 4, 14–34, Aug. 2012.
24. Wong, H., K. Luk, C. H. Chan, Q. Xue, K. K. So, and H. W. Lai, "Small antennas in wireless communications," *Proceedings of the IEEE*, Vol. 100, No. 7, 2109–2121, Jul. 2012.
25. Croq, F. and D. M. Pozar, "Millimeter-wave design of wide-band aperture-coupled stacked microstrip antennas," *IEEE Transactions on Antennas and Propagation*, Vol. 39, No. 12, 1770–1776, Dec. 1991.
26. Targonski, S. D., R. B. Waterhouse, and D. M. Pozar, "Design of wide-band aperture-stacked patch microstrip antennas," *IEEE Transactions on Antennas and Propagation*, Vol. 46, No. 9, 1245–1251, Sep. 1998.
27. Quijano, J. L. A. and G. Vecchi, "Optimization of an innovative type of compact frequency-reconfigurable antenna," *IEEE Transactions on Antennas and Propagation*, Vol. 57, No. 1, 9–18, Jan. 2009.
28. Quijano, J. L. A. and G. Vecchi, "Optimization of a compact frequency- and environment-reconfigurable antenna," *IEEE Transactions on Antennas and Propagation*, Vol. 60, No. 6, 2682–2689, Jun. 2012.
29. Rodríguez, D. O., M. A. Saavedra, G. A. Ramírez, and J. L. Araque, "Realization of a compact reconfigurable antenna for mobile communications," *2014 IEEE-APS Topical Conference on Antennas and Propagation in Wireless Communications (APWC)*, 284–287, Aug. 2014.
30. Arroyave, G. A. R. and J. L. A. Quijano, "Dual-port reconfigurable planar antennas for diversity and duplexing applications," *2016 IEEE International Symposium on Antennas and Propagation (APSURSI)*, 1247–1248, Jun. 2016.
31. Byndas, A., R. Hossa, M. E. Bialkowski, and P. Kabacik, "Investigations into operation of single- and multi-layer configurations of planar inverted-F antenna," *IEEE Antennas and Propagation Magazine*, Vol. 49, No. 4, 22–33, Aug. 2007.
32. Huynh, M. and W. Stutzman, "Ground plane effects on planar inverted-F antenna (PIFA) performance," *IEE Proceedings — Microwaves, Antennas and Propagation*, Vol. 150, No. 4, 209–213, Aug. 2003.
33. Best, S. R., "The significance of ground-plane size and antenna location in establishing the performance of ground-plane-dependent antennas," *IEEE Antennas and Propagation Magazine*, Vol. 51, No. 6, 29–43, Dec. 2009.
34. Anguera, J., A. Andújar, M.-C. Huynh, C. Orlenius, C. Picher, and C. Puente, "Advances in antenna technology for wireless handheld devices," *International Journal of Antennas and Propagation*, Vol. 2013, No. 1, 1–25, 2013, [online], available: https://doi.org/10.1155/2013/838364.

35. Anguera, J., C. Picher, A. Bujalance, and A. Andújar, "Ground plane booster antenna technology for smartphones and tablets," *Microwave and Optical Technology Letters*, Vol. 58, No. 6, 1289–1294, 2016, [online], available: https://onlinelibrary.wiley.com/doi/abs/10.1002/mop.29788.
36. Yoon, H. S. and S. O. Park, "A dual-band internal antenna of PIFA type for Bluetooth/WLAN in mobile handsets," *2007 IEEE Antennas and Propagation Society International Symposium*, 665–668, Jun. 2007.
37. Serra, A. A., P. Nepa, G. Manara, and R. Massini, "A low-profile linearly polarized 3D PIFA for handheld GPS terminals," *IEEE Transactions on Antennas and Propagation*, Vol. 58, No. 4, 1060–1066, Apr. 2010.
38. Khan, P., A. Abdullah Al-Hadi, P. J. Soh, M. T. Ali, S. S. Al-Bawri, and Owais, "Design and optimization of a dual-band sub-6 GHz four port mobile terminal antenna performance in the vicinity of user's hand," *Progress In Electromagnetics Research C*, Vol. 85, 141–153, 2018.
39. Nguyen-Trong, N., A. Piotrowski, and C. Fumeaux, "A frequency-reconfigurable dual-band low-profile monopolar antenna," *IEEE Transactions on Antennas and Propagation*, Vol. 65, No. 7, 3336–3343, Jul. 2017.
40. Wang, D., G. Wen, and Q. Rao, "A 3D compact pent-band antenna for wireless mobile communication," *2008 IEEE Antennas and Propagation Society International Symposium*, 1–4, Jul. 2008.
41. Li, G., H. Zhai, T. Li, X. Y. Ma, and C.-H. Liang, "Design of a compact UWB antenna integrated with GSM/WCDMA/WLAN bands," *Progress In Electromagnetics Research*, Vol. 136, 409–419, 2013.
42. Alibakhshikenari, M., B. S. Virdee, and E. Limiti, "Triple-band planar dipole antenna for omnidirectional radiation," *Microwave and Optical Technology Letters*, Vol. 60, No. 4, 1048–1051, 2018, [online], available: https://onlinelibrary.wiley.com/doi/abs/10.1002/mop.31098.
43. Alibakhshikenari, M., B. S. Virdee, A. Ali, and E. Limiti, "Miniaturised planar-patch antenna based on metamaterial L-shaped unit-cells for broadband portable microwave devices and multiband wireless communication systems," *IET Microwaves, Antennas Propagation*, Vol. 12, No. 7, 1080–1086, 2018.
44. Alibakhshikenari, M., E. Limiti, M. Naser-Moghadasi, B. S. Virdee, and R. Sadeghzadeh, "A new wideband planar antenna with band-notch functionality at GPS, Bluetooth and WiFi bands for integration in portable wireless systems," *AEU — International Journal of Electronics and Communications*, Vol. 72, 79–85, 2017, [online], available: http://www.sciencedirect.com/science/article/pii/S1434841116309955.
45. Sravani, P. and M. Rao, "Design of 3D antennas for 24 GHz ISM band applications," *2015 28th International Conference on VLSI Design*, 470–474, Jan. 2015.
46. Menéendez, L. G., O. S. Kim, F. Persson, M. Nielsen, and O. Breinbjerg, "3D printed 20/30-GHz dual-band offset stepped-reflector antenna," *2015 9th European Conference on Antennas and Propagation (EuCAP)*, 1–2, Apr. 2015.
47. Gjokaj, V., P. Chahal, J. Papapolymerou, and J. D. Albrecht, "A novel 3D printed Vivaldi antenna utilizing a substrate integrated waveguide transition," *2017 IEEE International Symposium on Antennas and Propagation USNC/URSI National Radio Science Meeting*, 1253–1254, Jul. 2017.
48. Jofre, L., B. A. Cetiner, and F. D. Flaviis, "Miniature multi-element antenna for wireless communications," *IEEE Transactions on Antennas and Propagation*, Vol. 50, No. 5, 658–669, May 2002.
49. Harrington, R., "On the gain and beamwidth of directional antennas," *IRE Transactions on Antennas and Propagation*, Vol. 6, No. 3, 219–225, Jul. 1958.
50. Ramírez Arroyave, G. A. and J. L. Araque Quijano, "Broadband characterization of 3D printed samples with graded permittivity," *2018 International Conference on Electromagnetics in Advanced Applications (ICEAA)*, 584–588, Sep. 2018.
51. Arroyave, G. A. R. and J. L. A. Quijano, "Evaluation of additive manufacturing processes for 3-D multiband antennas," *2018 International Conference on Electromagnetics in Advanced Applications (ICEAA)*, 589–592, Sep. 2018.